J Electroceram (2012) 29:99–105
DOI 10.1007/s10832-012-9751-2

Synthesis and electric characterization of rare earth double perovskite Ho_2CdZrO_6 ceramics

Dev K. Mahato · A. Dutta · T. P. Sinha

Received: 30 December 2011 / Accepted: 22 June 2012 / Published online: 13 July 2012

Abstract A new double perovskite oxide holmium cadmium zirconate Ho_2CdZrO_6 (HCZ) is synthesized by solid state reaction technique. The crystal structure has been determined by powder X-ray diffraction (XRD) which shows monoclinic phase at room temperature. The frequency dependent electrical data are analyzed in the framework of conductivity and electric modulus formalisms. The scaling behavior of imaginary electric modulus suggests that the relaxation describe the same mechanism at various temperatures. Nyquist plots are drawn to identify an equivalent circuit and to know the bulk and interface contributions. The conduction mechanism is explained by Mott's theory. At the high temperature range, conductivity data satisfy the variable range hopping (VRH) model. In this regime, the conductivity of sample obeys Mott's $T^{1/4}$ law indicating 3D charge transport in HCZ compound. High temperature data indicates the formation of thermally activated small polarons.

Keywords Chemical synthesis · Double perovskite · Electrical properties

1 Introduction

Double perovskites, with general formula $A_2B'B''O_6$, are one of the most widely studied families of oxides owing greatly to their synthetic variability, compositional flexibility and intriguing properties. Double perovskite compounds have attracted a great deal of researchers' interest due to their extraordinary transport properties [1–6] as a result of different possible electrons that can occupy the A, B′ and B″-site. In these oxides, one kind of octahedral in the structure is $B'O_6$ and the other is $B''O_6$. For the octahedra to be distinct there must usually be a large difference in size and charge between B′ and B″. The two kind of octahedra in the double perovskite structure are arranged as in the rock salt where the B′ and B″ cations are alternately ordered. The physical properties of interest among double perovskites include superconductivity, colossal magnetoresistance, ionic conductivity and a multitude of dielectric properties, which are of great importance in microelectronics and telecommunication. Because of the great flexibility inherent in the perovskite structure [7, 8] there are many different types of distortions which can occur from the ideal structure. Many of the physical properties of double perovskites depend crucially on the details of these distortions, particularly the electronic, magnetic and dielectric properties which are so important for many of the applications of double perovskites. Recently, the study of these perovskite materials has increased due to the possibility of applying them in the design and development of tunnel junctions, magnetic memories and several other technologically important magnetic devices in the novel spintronics area [9].

The rare earth oxides have many applications in solid-state electronics, electrical and transparent opto-ionic devices. The basic promise of rare earth oxides in electronics is that of enabling high temperature and high-power devices. These oxides have high resistivity, high dielectric constant, large band gap, high recrystallization temperature and thermodynamically stable in contact with Si substrate at high temperature (~800 °C) under high vacuum [10]. Since most of the devices are operated in the ac electrical mode, the investigation of ac electrical conduction of these materials is interesting.

Though the electrical properties of various double perovskites have been studied in the recent past [11–15], no

D. K. Mahato (✉)
Department of Physics, National Institute of Technology Patna,
Patna 800 005, India
e-mail: drdevkumar@yahoo.com

A. Dutta · T. P. Sinha
Department of Physics, Bose Institute,
93/1, Acharya Prafulla Chandra Road,
Kolkata 700 009, India

attempt has so far been made to study the perovskite Ho_2CdZrO_6. In this paper we, therefore, report the preparation and electrical properties of a new double perovskite oxide Ho_2CdZrO_6 in a frequency range (100 Hz–1 MHz) at various temperatures.

2 Experimental

The sample Ho_2CdZrO_6 (HCZ) was prepared through solid state reaction route. Powders of Ho_2O_3 (Aldrich, 99.9 %), CdO (Loba Chemie, 99 %) and ZrO_2 (Loba Chemie, reagent grade, 99.5 %) were taken as primary raw materials and stoichiometrically mixed in a agate mortar in the presence of acetone (Merck) for 12 h. The mixture was calcined in a Pt crucible at 1100 °C in air for 10 h and brought to room temperature at a cooling rate of 100 °C/h. The calcined sample was palletized into a circular disc (of thickness 1 mm and diameter 10 mm) using PVA as binder which was burnt out during high temperature sintering at 1150 °C for 6 h, and cooled slowly to room temperature at a cooling rate 1 °C/min. The sample was characterized by X-ray diffraction pattern and scanning electron micrograph. The X-ray diffractogram of the sample was recorded at room temperature with Rigaku Miniflex-II automatic X-ray powder diffractometer in a wide range of Bragg angles ($10° \leq 2\theta \leq 80°$) using CuK$\alpha$ radiation (λ=1.5418 Å) and a Ni filter operating at 30 kV and 15 mA at a scanning rate of 2°/min. The scanning electron microscope (FEI Quanta 200) was used to determine the grain size distribution.

The sintered pellets were polished to make both their faces parallel and electroded by high purity ultrafine silver paste for all their electrical characterization. To dry the paste the samples were evaporated onto both sides of the disc at 500 °C for 2 h prior to conducting experiment. Capacitance (C), impedance (Z), phase angle(φ) and conductance (G), of the sample were measured in a wide frequency range (100 Hz to 1 MHz) at various temperature using a computer controlled LCR-meter (HIOKI-3552, Japan) at a heating rate of 0.5 °C/min. The Eurotherm 2216e temperature controller was used to control the temperature of the sample.

3 Results and discussion

3.1 Structural characterization

The X-ray diffraction pattern of HCZ measured at room temperature is shown in Fig. 1. The pattern is characteristic of a perovskite structure. All the reflection peaks of the X-ray profile are indexed and lattice parameters are determined using a least-squares method with the help of a standard computer programme (Crysfire). Good agreement between the observed and calculated interplanner spacing (d-values), Table 1, suggests that the compound crystallizes in monoclinic phase at room temperature. The cell parameters are a= 8.6134±0.0028 Å, b=6.4611±0.0041 Å, c=6.2778± 0.0018 Å and β=94.0732±0.0401° with cell volume V= 348.49 $Å^3$. X-ray diffraction confirms that the specimen is single phase. A SEM image of the sample is shown in the inset of Fig. 1. The SEM image indicates the uniformity of the grains in the samples. The grain size of HCZ is found to be in the range 0.61–1.39 μm.

3.2 Electric modulus analysis

An alternative approach to investigate the dynamical aspects of electrical transport phenomena of materials is the complex electric modulus $M^*(\omega)$. The electrode polarization effect is minimized in this representation. The complex electric modulus is represented by the following expression [16]:

$$M^*(\omega) = 1/\varepsilon^* = i\omega C_0 Z^* = M'(\omega) + iM''(\omega) = M_\infty \left[1 - \int_0^\infty \exp(-i\omega t)\left\{\frac{d\phi(t)}{dt}\right\}dt\right] \quad (1)$$

Where C_0 is the vacuum capacitance of the cell and ε^* is the complex permittivity, M' and M'' represent the real and imaginary parts of complex electric modulus (M^*).

$M_\infty = 1/\varepsilon_\infty$, M_∞(high frequency asymptotic value of M') and ε_∞ is the high frequency asymptotic value of the real part of the dielectric permittivity and $\varphi(t)$ is the relaxation function, which gives the time evolution of the electric field within the materials. Figure 2(a) and (b) shows the frequency dependence of the real $M'(\omega)$ and imaginary $M''(\omega)$ parts of the complex electric modulus (M^*) of HCZ at various temperatures. The real part of electric modulus $M'(\omega)$ shows a dispersion tending towards M_∞ (high frequency asymptotic value of M') i.e. at high frequencies, $M'(\omega)$ approaches a maximum M_∞ and at low frequencies M' approaches to zero indicates that the electrode polarization makes a negligible low contribution to M' [17]. The dispersion in between low and high frequencies is due to the conductivity relaxation. At higher temperatures and at higher frequencies, M_∞ levels off because the relaxation processes are spread over a range of frequencies. The peaks developed in the values of imaginary parts of electric modulus $M''(\omega)$ indicate a relaxation process. The peak position shifts towards higher frequency side with an increase of temperature indicating the thermally activated nature of the relaxation time. Two apparent relaxation regions appear the region towards left of the peak associated with the conduction process where the charge carriers are mobile over a long distance; the region towards right of the peak associated with the relaxation polarization process where the charge carriers are spatially confined to

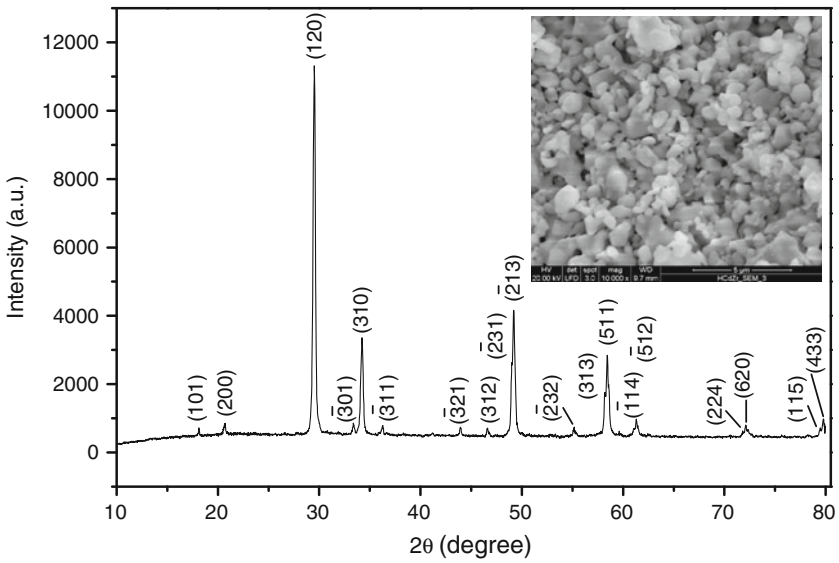

Fig. 1 XRD pattern of Ho_2CdZrO_6 at room temperature. Inset: a SEM image of the sintered pellet of Ho_2CdZrO_6

the potential wells. We have fitted our experimental data to Eq. (2) as shown by solid lines in Fig. 2(b) with the Cole-Cole expression defined as [18]:

$$M'' = \frac{M_\infty M_s[(M_\infty - M_s)\sin\varphi]A}{M_s^2A^2 + 2A(M_\infty - M_s)M_s\cos\varphi + (M_\infty - M_s)^2}, \quad (2)$$

where, $A = \left[1 + 2(\omega\tau^{1-\alpha})\sin(\alpha\pi/2) + (\omega\tau)^{2(1-\alpha)}\right]^{1/2}$ and $\varphi = \tan^{-1}\left[(\omega\tau)^{1-\alpha}\cos(\alpha\pi/2)/\left[1 + (\omega\tau)^{1-\alpha}\sin(\alpha\pi/2)\right]\right]$.

The value of α is lying in between 0.10 and 0.18 for the temperatures ranging from 30 to 270 °C.

The temperature dependence of the characteristic relaxation time $\tau_m\left(=\omega_m^{-1}\right)$ is shown in the inset of Fig. 3, which also obeys the Arrhenius law and the corresponding activation energy is E_a=0.23 eV (E_a represents activation energy obtained from the peak position of M'' versus logω plots).

Table 1 Comparision of observed and calculated d-values (Å) of some reflection of HCZ compound at room temperature

2θobs (deg.)	h k l	d_{obs} (Å) (a)	d_{cal} (Å) (b)	Diff. (a-b)	I/Io
18.120	101	4.8971	4.8958	0.0013	2
20.640	200	4.2957	4.2941	0.0016	3
29.500	120	3.0255	3.0229	0.0026	100
33.380	-301	2.6822	2.6763	0.0059	3
34.240	310	2.6179	2.6172	0.0007	27
36.240	-311	2.4768	2.4725	0.0043	3
43.900	-321	2.0607	2.0607	0.0000	3
46.580	312	1.9474	1.9465	0.0009	2
49.000	-231	1.8575	1.8563	0.0012	24
49.200	-213	1.8504	1.8504	0.0000	39
55.140	-232	1.6638	1.6632	0.0006	2
58.200	313	1.5839	1.5827	0.0012	15
58.440	511	1.5780	1.5779	0.0001	26
61.040	-114	1.5164	1.5156	0.0008	3
61.300	-512	1.5110	1.5100	0.0010	5
71.800	224	1.3137	1.3135	0.0002	2
72.100	620	1.3089	1.3086	0.0003	5
79.460	115	1.2054	1.2049	0.0005	2
79.780	433	1.2011	1.2003	0.0008	4

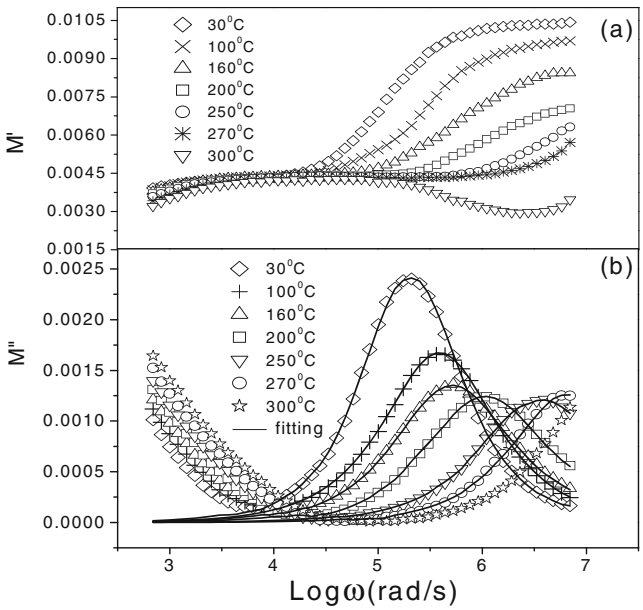

Fig. 2 Frequency dependence of (**a**) M′ and (**b**) M″ of Ho_2CdZrO_6 at various temperatures where symbols are the experimental points and solid lines are the fitting to Eq. (2) as shown in Fig. 2b

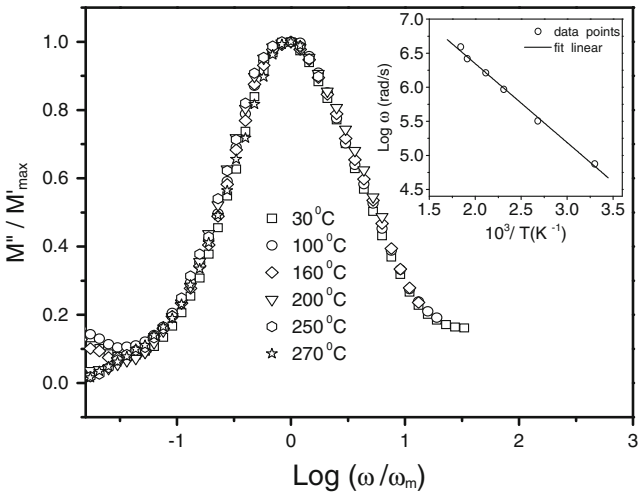

Fig. 3 Scaling behaviour of M″ at various temperatures for Ho_2CdZrO_6. Inset: The temperature dependence of the most probable relaxation frequency obtained from the frequency-dependent plot of M″, symbols are the experimental points and the solid line is the least-squares straight line fit

Such a value of activation energy suggests the existence of a relaxation mechanism (a conductive process), which may be interpreted as polaron hopping between neighboring sites within the crystal lattice. In order to mobilize the localized electron, the aid of lattice oscillation is required. In these circumstances, electrons are considered not to move by themselves but by hopping motion activated by lattice oscillation i.e. the conduction mechanism is considered as phonon-assisted hopping of small polaron between localized states.

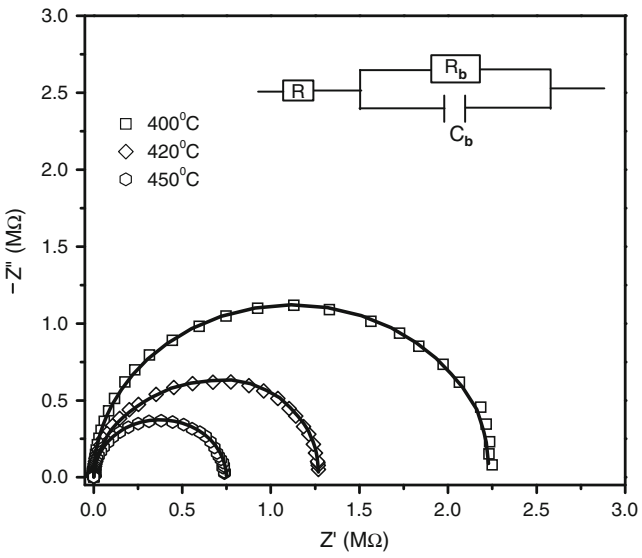

Fig. 4 Complex plane plot of impedance for Ho_2CdZrO_6 at 400 °C, 420 °C and 450 °C, solid line is the fitting to the experimental data by RC equivalent circuit

The scaling behaviour of M'' i.e. M''/M''_{max} versus log (ω/ω_{max}) plot of HCZ at various temperatures is shown in Fig. 3. The overlapping of the curves for all the temperatures into a single master curve indicates that the dynamical processes are nearly temperature independent.

3.3 Impedance study

The electrical properties of the material were determined by impedance spectroscopy. Experimental complex impedance data may well be approximated by the impedance of an equivalent circuit consists of resistors, capacitors and possibly various distributed circuit elements. These equivalent circuit can be physically interpreted and assign them to appropriate process. The display of impedance data in complex plane plot appears in the form of a succession of semicircles attributed to relaxation phenomena with different time constants due to the contribution of grain (bulk), grain-boundary and interface/electrode polarization in the polycrystalline materials. Hence the contribution to the overall electrical properties by various components in the material is separated out easily. Figure 4 shows a typical complex impedance plane plot and the corresponding equivalent circuit of HCZ at 400, 420 and 450°C. The impedance spectrum shows only one high frequency semicircular arc, and the semicircular arc becomes smaller with increasing temperature. The high frequency semicircular arc corresponds to bulk property of the material arising due to parallel combination of bulk resistance (R_b) and bulk capacitance (C_b) of the material (inset of Fig. 4). The complex impedance (Z*) for the equivalent circuit in this system is

$$Z^* = Z' - iZ'' = R + \frac{1}{R_b^{-1} + i\omega C_b}$$

Where R is the series resistance, Z′ and Z″ are the real and imaginary parts of complex impedance given by:

$$Z' = R + \frac{R_b}{1 + (\omega R_b C_b)^2} \tag{3}$$

and

$$Z'' = R_b\left[\frac{\omega R_b C_b}{1 + (\omega R_b C_b)^2}\right] \tag{4}$$

We have fitted our experimental data with Eqs. (3) and (4) as shown by solid lines in Fig. 4. The fitted parameters for R_b are 2.24 MΩ, 1.27 MΩ and 0.75 MΩat temperatures 400, 420 and 450°C respectively, and the corresponding bulk capacitance (C_b) values are 4.87×10^{-11} F, 4.95×10^{-11} F, 5.81×10^{-11} F. A good agreement between the experimental and fitted data indicates that the polarization mechanism correspond to the bulk effect arising from the semiconductive grains.

3.4 Electrical conductivity

AC conductivity measurement is an important tool for studying the transport properties of materials. The conductivity is found to be frequency independent in low frequency region and is illustrated as dc conductivity. The temperature dependence of the dc conductivity gives information about the long time charge carrier dynamics and it is well described by the Arrhenius law, reflecting the activated nature of hopping processes. At high frequencies, the conductivity becomes strongly frequency dependent, varying approximately as a fractional power of frequency. Full analysis of this dispersion not only required accurate data but also appropriate model to represent the response. We have taken Jonscher's power law for ac conductivity analysis. The frequency dependence of real part of ac conductivity $\sigma'(\omega)$ at various temperatures for HCZ is shown in Fig. 5. The real part of conductivity $\sigma'(\omega)$ shows dispersion that shifts to the higher frequency side with increasing temperature. From Fig. 5 it is clear that $\sigma'(\omega)$ decreases with decreasing frequency and becomes frequency independent after a certain value (i.e. in low frequency region) giving dc conductivity (σ_{dc}). The value of σ_{dc} is found to increase with an increase of temperature. For higher frequencies power-law behaviour, $\sigma'(\omega) \sim A\omega^n$ is observed. The ac conductivity spectra then can be described by the so-called Jonscher's universal power law [19] defined as:

$$\sigma'(\omega) = \sigma_{dc} + \sigma_{ac}(\omega) = \sigma_{dc} + A\omega^n \tag{5}$$

Where $\sigma'(\omega)$, σ_{dc}, $\sigma_{ac}(\omega)$ have their usual meanings, A is a constant and n is the frequency exponent lies in the range $0<n<1$. The term $A\omega^n$ comprises the ac dependence and characterizes all dispersion phenomena. The experimental conductivity data of HCZ are fitted to Eq. (5) keeping in mind that the values of parameter n are weakly temperature dependent. The best fit of conductivity spectra is shown by solid lines in Fig. 5 with values of n are 0.88–0.92 for temperatures 350–450 °C. There is a vast number of theoretical approaches to deduce this behavior from the microscopic transport properties of various classes of materials [20]. The quantum-mechanical tunneling model, which corresponds to the variable range hopping (VRH) model for nonzero frequencies, predicts a temperature-independent frequency exponent n near 0.8 [20].

Typical plot of temperature variations of log of dc conductivity σ_{dc} for HCZ is shown in Fig. 6. It is obvious that the σ_{dc} increases with increasing temperature showing the semiconducting behaviour of the material. This semiconducting behavior can also be observed in Fig. 5 at lower frequencies. To understand the mechanism of electrical conduction, we have analyzed the conductivity data in terms of small polaron hopping and variable range hopping (VRH) models [21, 22].

The temperature dependence of the dc conductivity σ_{dc} is shown in Fig. 7. The results indicate that $\sigma_{dc}(T)$ cannot be fitted assuming a thermally activated conduction mechanism, which is commonly used to characterize band conduction. The dc conductivity [22] in semiconductors, in which the main conduction mechanism is related to excited carriers beyond the mobility edge into the non-localized or extended states, is expressed as:

$$\sigma_{dc} = \sigma_o \exp\left[\frac{-E_a}{k_B T}\right] \tag{6}$$

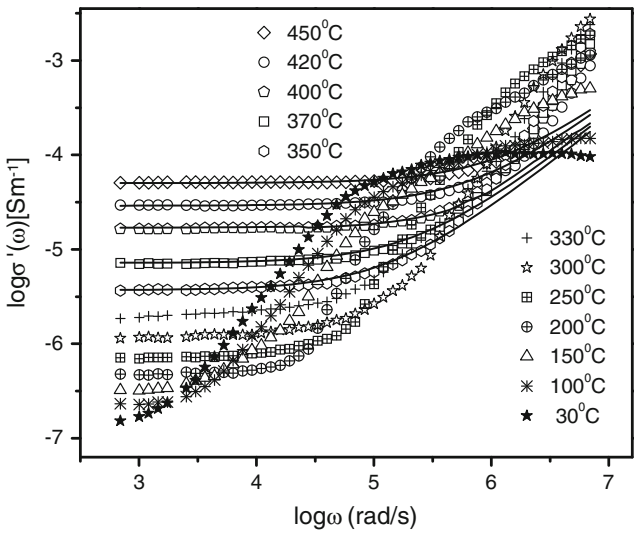

Fig. 5 Frequency dependence of the conductivity (σ) for Ho_2CdZrO_6 at various temperatures, symbols are the experimental points and solid lines represent the fitting of Jonscher's power law

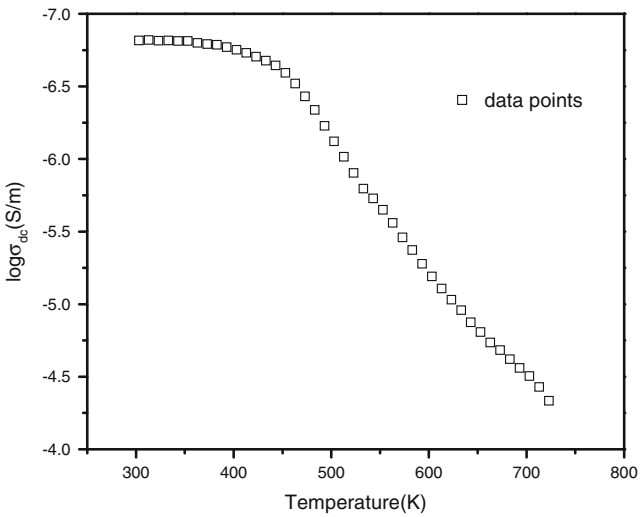

Fig. 6 Temperature variation of electrical conductivity for Ho_2CdZrO_6

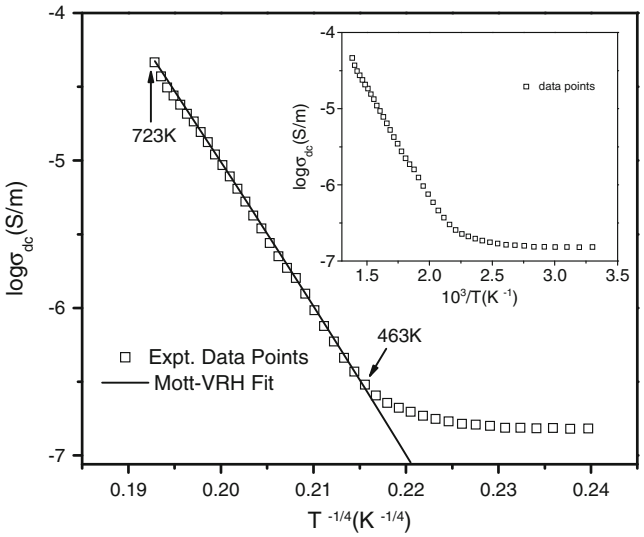

Fig. 7 Temperature dependence of dc conductivity for Ho_2CdZrO_6: log σ_{dc} versus $T^{-1/4}$. The symbols are the experimental points and the solid line is fit to Mott-VRH prediction, Eq. (7). Inset shows the data in Arrhenius representation

where, σ_0 is the pre-exponential factor, E_a the activation energy for conduction, k_B the Boltzmann constant and T is the Kelvin temperature. The Arrhenius plot shown in the inset of Fig. 7 does not lead to straight line over significant temperature ranges. The slight curvature in the conductivity log σ_{dc} vs. T^{-1} plot occurred within the low temperature range. Such a curvature in the plot suggested that the variable range hopping (VRH) of small polaron model could be concerned in such a case. The variable range hopping of small polaron conductivity model described the conductivity with the formula [21–25]:

$$\sigma_{dc} = \sigma_0 \exp\left[-(T_0/T)^{1/4}\right] \tag{7}$$

$$T_0 = \frac{16}{k_B N(E_F) L^3} \tag{8}$$

where $N(E_F)$ is the density of localized states at the Fermi level, L the localization length and T_0 is the Mott's characteristic temperature. The experimental data were fitted satisfactorily by solid line to Eq. (7) in the temperature range (~463–723 K) with $T_0 = 5.2 \times 10^7 K$ was obtained from fit as shown in Fig. 7. The reported value of $N(E_F)$(=5.68×10^{17} eV^{-1} cm^{-3}) [21, 22, 24, 25] yields a location length L of the order of 18 Å for HCZ as calculated from Eq. (8). This value of location length L is found to be in the same order of magnitude as reported by Mahato et al. [6, 24] for double perovskite oxides. The average hopping distance, $R_h(T)$ between two localized states and hopping energy, $E_h(T)$, are given by the following equations [22]:

$$R_h(T) = \left(\frac{3}{8}\right) L \left(\frac{T_0}{T}\right)^{1/4} \tag{9}$$

and,

$$E_h(T) = \left(\frac{1}{4}\right) k_B T \left(\frac{T_0}{T}\right)^{1/4} \tag{10}$$

The calculated values of R_h(300 K) and E_h(300 K) are 13.8 nm and 0.132 eV respectively. It is evident from Fig. 7 that the plot log σ_{dc} vs. $1/T^{1/4}$ leads to straight line over a considerable temperature range (463–723 K) i.e. Mott's law is obeyed over a temperature range 463–723 K and indicates 3D charge transport in HCZ compound. Below 463 K, it was observed that conductivity data deviate from the straight line behaviour because in low temperature region charge conduction is mainly dominated by the thermally stimulated tunneling through the localized sites. Therefore the observed dc conductivity is contributed as the sum of hopping conduction and tunneling conduction. Band conduction is absent because the extended states are far away from the Fermi level. Such a deviation from linearity at lower temperature has also been observed by Molak et al. [26] and explained with the help of variable range hopping of small polaron model.

Figure 7 also suggests that a change in conductivity mechanism likely occurs near 463 K. Above 463 K the conductivity is associated with polaron transport in the extended states at the mobility edge. At temperatures nearing 463 K the probability of thermal release becomes rapidly smaller, which makes polaron hops to a neighbouring localized state more likely to take place below 463 K.

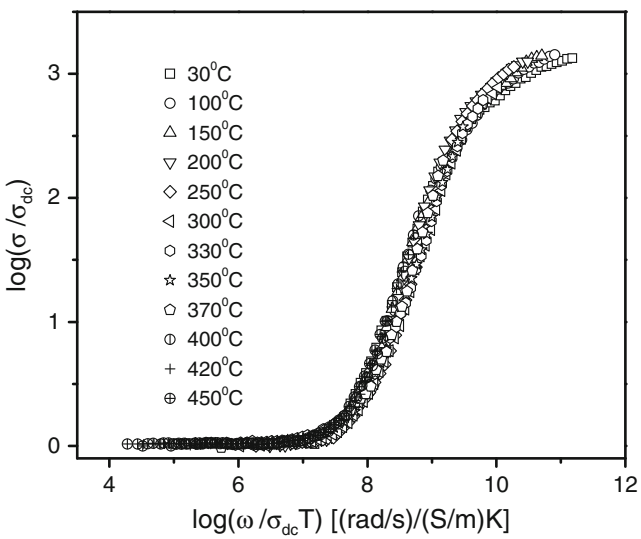

Fig. 8 Relation between $\log(\sigma_{ac}/\sigma_{dc})$ and $\log(\omega/\sigma_{dc}T)$ at different temperatures for Ho_2CdZrO_6

3.5 ac conductivity scaling studies

We have performed a scaling process of the a.c. conductivity as a function of frequency as shown in Fig. 8, which shows the conductivity master curves of the sample HCZ. In Fig. 8 we have used log (σ_{ac}/σ_{dc}) as the y-axis scaling parameter and log ($\omega/\sigma_{dc}T$) as the x-axis parameter at different temperatures. This scaling was proposed by Rolling et al. [27] where it was found that the product $T\sigma_{dc}$ obeys an Arrhenius relation. From Fig. 8, it is clear that a quite satisfying overlap of the data at different temperatures on a single master curve illustrates well the dynamic processes occurring at different frequencies need almost the same thermal activation energy. Another indication of those scaled master curves is that all Arrhenius temperature dependence of conductivity is embedded in the d.c. conductivity term [28].

4 Conclusions

In this work, we have reported the electrical modulus and electric conduction mechanism in double perovskite oxide Ho_2CdZrO_6 (HCZ) synthesized by solid state reaction route. The X-ray diffraction analysis shows monoclinic phase at room temperature. The activation energy (0.23 eV) obtained from M'' peaks suggests that the conduction mechanism in HCZ may be due to the polaron hopping based on the electron carriers. Frequency dependent conductivity for HCZ obeys Jonscher's power law with high frequency dispersion. The variation of dc conductivity with temperature indicates the semiconducting nature of the material. The conduction mechanism is explained by Mott's theory and Mott's parameters were determined. From the temperature-dependent conductivity investigation we concluded that the three-dimensional type variable range hopping conduction is the dominant mechanism. The a.c. scaling study suggests that the conductivity relaxation mechanism is independent of temperature.

Acknowledgements This work is financially supported by Department of Science and Technology of India under grant no. SR/S2/CMP-01/2008.

References

1. K.I. Kobayashi, T. Kimura, H. Swada, K. Terakura, Y. Tokura, Nature (London) **395**, 677 (1998)
2. F. Zhao, Z. Yue, Z. Gui, L. Li, Japn J. Appl. Phys. **44**, 8066 (2005)
3. C. Vijaykumar, H.P. Kumar, V.T. Kavitha, S. Solomon, J.K. Thomas, P.R.S. Wariar, J. Koshy, J. Alloy. Compd. **475**, 778 (2009)
4. R. Kumar, C.V. Tomy, R. Nagarajan, P.L. Paulose, S.K. Malik, Physica B **404**, 2369 (2009)
5. A. Dutta, T.P. Sinha, S. Shannigrahi, Japn. J. Appl. Phys. **49**, 061504 (2010)
6. D.K. Mahato, A. Dutta, T.P. Sinha, Solid State Sciences **14**(1), 21 (2012)
7. P.J. Saines, B.J. Kennedy, M.M. Elcombe, Solid state Chem **180**, 401 (2007)
8. B. Raveau, Prog. Solid State Chem. **35**, 171 (2007)
9. C. Li, X. Junmin, J. Wang, J. Electroceram **16**, 351 (2006)
10. A.A. Dakhel, Cryst. Res. Technol. **39**(5), 404 (2004)
11. A. Sellai, H. Widatallah, O.A. Yassin, M. Elzain, Key Engg. Mater. **150**, 368 (2008)
12. S. Tao, J.T.S. Irvine, J. Mater. Chem. **12**, 2356 (2002)
13. K.L. Holman, Q. Huang, T. Klimczuk, K. Trzebiatowski, J.W.G. Bos, E. Morosan, J.W. Lynn, R.J. Cava, J. Solid State Chem. **180**, 75 (2007)
14. A. Dhahri, J. Dhahri, M. Oumezzine, Mater. Lett. **63**, 121 (2009)
15. M. Zazo, A.G. Flores, J. Iniguez, L. Torres, J. Appl. Phys. **89**(11), 7642 (2001)
16. J.R. Macdonald, Solid State Ionics **133**, 79 (2000); J.R. Macdonald, J. Appl. Phys. **90**, 153 (2001)
17. A.K. Himanshu, B.K. Choudhary, D.C. Gupta, S.K. Bandhopadhayay, T.P. Sinha, Physica B **405**, 1608 (2010)
18. G.M. Tsangaris, G.C. Psarras, N. Kouloumbi, J. Mater. Sci. **33**, 2027 (1998)
19. A.K. Jonscher, *Dielectric Relaxation in Solids* (Chelsea Dielectric Press, London, 1983)
20. S.R. Elliot, Adv. Phys. **36**, 135 (1987); A.R. Long, ibid. **31**, 553 (1982)
21. N.F. Mott, *Metal-Insulator Transitions* (Taylor & Francis, London, 1990)
22. N.F. Mott, E.A. Davis, *Electronic Processes in Non-crystalline Marerials* (Clarendon, Oxford, 1971)
23. A.G. Hunt, Philos. Mag. B **81**, 875 (2001)
24. A. Banerjee, S. Pal, E. Rozenberg, B.K. Chaudhuri, J. Phys. Condens. Matter **13**, 9489 (2001)
25. R.N. Mahato, K. Sethupathi, V. Sankaranarayanan, K.K. Bharathi, R. Nirmala, A.K. Nigam, S.K. Malik, IEEE Trans. Magn. **43**(10]), 4271 (2009)
26. A. Molak, M. Paluch, S. Pawlus, Z. Ujma, M. Pawelczyk, I. Gruszka, Phase Transition **79**, 447 (2006); A. Molak, M. Pawelczyk, Ferroelectrics **367**, 179 (2008)
27. B. Roling, A. Happe, K. Phunke, M.D. Ingram, Phys. Rev. Lett. **78**, 2160 (1997); B. Roling, Phys. Chem. Chem. Phys. **3**, 5093 (2001)
28. S.A. Safan, Physica B: Condens. Matter **403**, 2049 (2008)